Molecular-Level Interactions of Nanodisc-Forming Copolymers Dissected by EPR Spectroscopy

Jana Eisermann, Matthias Hoffmann, Florian A. Schöffmann, Manabendra Das, Carolyn Vargas, Sandro Keller, and Dariush Hinderberger*

This study focuses on analyzing the noncovalent interaction patterns between three lipid-nanodisc-forming polymers and nitroxide radicals which are used as small organic tracer molecules. Besides the negatively charged polymers diisobutylene/maleic acid (DIBMA) and styrene/maleic acid (SMA) (2:1), the solvation behavior of a newly synthesized zwitterionic styrene/maleic amide sulfobetaine copolymer named SMA-sulfobetaine (SB) is characterized. The applied spin probes vary in their respective chemical structure, allowing the report of different local micropolarities and nanoscopic regions by recording temperature-dependent continuous-wave electron paramagnetic resonance (CW EPR) spectra. In combination with light scattering experiments, a nanoscopic interpretation of the dominant polymer/guest molecule interaction patterns is provided. The results indicate that in SMA and DIBMA, ionic interactions dominate the interaction patterns with other molecules. In SMA-SB, the zwitterionic side chains mainly induce a dynamic assembly with guest molecules due to weaker noncovalent interactions. Depending on the applied spin probe, temperature-dependent CW EPR measurements reveal nanoscopic cloud points depending on the interaction patterns with SMA-SB which can occur more than 20 °C below its macroscopically observed upper critical solution temperature. Finally, the detailed dissection of interaction patterns may provide a better understanding that may even allow tuning the polymers' properties for use in lipid nanodisc formation.

1. Introduction

In recent years, remarkable progress has been made in the development and understanding of lipid model membrane systems that are alternatives to classical liposomes. Polymer-encapsulated nanodiscs, also known as native nanodiscs, lipodisqs, or polymer/lipid particles, are considered one of the most promising candidate systems for studying lipid/lipid, lipid/protein, and protein/protein interactions. This is chiefly due to the small size of these nanodiscs and their compatibility with many commonly used biochemical, functional, and structural methods.[1–4] Another advantage of nanodisc-forming polymers is their capability of solubilizing lipids as well as target proteins directly from native membranes. Therefore, the use of these polymers enables researchers to purify membrane proteins without conventional detergents that may denature labile proteins.[1–3,5]

Despite their wide use, the understanding of the basic principles governing the interactions between polymers and small- or medium-sized amphiphilic molecules

Dr. J. Eisermann, M. Hoffmann, F. A. Schöffmann, Prof. D. Hinderberger
Institute of Chemistry–Physical Chemistry–Complex
Self-Organizing Systems
Martin Luther University (MLU) Halle-Wittenberg
Von-Danckelmann-Platz 4, 06120 Halle (Saale), Germany
E-mail: dariush.hinderberger@chemie.uni-halle.de

Dr. J. Eisermann
Department of Chemistry – Molecular Sciences Research Hub
Imperial College London
82 Wood Ln, London W12 0BZ, UK

M. Hoffmann, F. A. Schöffmann, Prof. D. Hinderberger
Interdisciplinary Research Center HALOmem
MLU Halle-Wittenberg
Charles Tanford Protein Center
Kurt-Mothes-Str. 3a, 06120 Halle (Saale), Germany

Dr. M. Das, C. Vargas, Prof. S. Keller
Molecular Biophysics
Technische Universität Kaiserslautern (TUK)
Erwin-Schrödinger-Str. 13, 67663 Kaiserslautern, Germany

C. Vargas, Prof. S. Keller
Department of Biophysics
Institute of Molecular Biosciences (IMB)
NAWI Graz
University of Graz
Humboldtstr, Graz 8010, Austria

C. Vargas, Prof. S. Keller
Field of Excellence BioHealth
University of Graz
Humboldtstr, 50/I, Graz 8010, Austria

C. Vargas, Prof. S. Keller
BioTechMed-Graz
Mozartstr, 12/II, Graz 8010, Austria
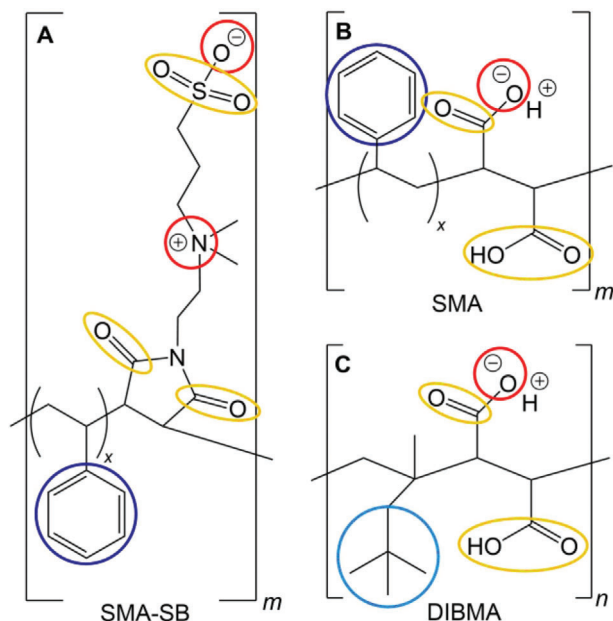
Figure 1. Molecular structures of the studied nanodisc-forming polymers A) SMA-SB and B) SMA with x = 2.2, m ≈ 8 as well as C) DIBMA with n ≈ 37. The colors mark different possible interaction sites as follows: red, ionic interactions; yellow, hydrogen bonding and dipole/dipole interactions; dark blue, π/π interactions; light blue, van der Waals interactions.

such as lipids has not developed as quickly as their applications. Continuous-wave electron paramagnetic resonance (CW EPR) spectroscopy has been developed into a powerful technique to locally analyze such structural, dynamic, and functional properties of the polymers on the molecular scale.[6–8] In this study, we characterize three types of nanodisc-forming polymers through their noncovalent interactions with EPR-active nitroxide radicals. These amphiphilic polymers encompass a 2:1 styrene/maleic acid copolymer (SMA (2:1)), a diisobutylene/maleic acid copolymer (DIBMA),[9,10] and a zwitterionic styrene/maleic amide sulfobetaine copolymer (SMA-SB) derived from SMA (2:1). The structures and properties of the studied polymers are shown in **Figure 1** and **Table 1**. The chosen spin probes are depicted in **Figure 2**; they vary in their chemical structure and can, therefore, report on different noncovalent interaction patterns, micropolarities, and nanostructured regions.[11–14]

Here, we characterize interactions between the shown spin probes (Figure 2) and three nanodisc-forming polymers (Figure 1 and Table 1) using CW EPR spectroscopy at X- and Q-band frequencies. The EPR-based view on the polymeric systems is com-

plemented by dynamic light scattering (DLS) and electrophoretic light scattering (ELS) experiments. By combining all results, we provide a nanoscopic interpretation of the dominant interaction patterns in polymer nanodisc systems. This detailed dissection of interaction patterns may aid in better understanding and even tuning the polymers' properties for use in lipid nanodisc formation.

2. Results and Discussion

2.1. Light Scattering

Prior to characterizing the polymers on the molecular level with EPR spectroscopy, their solvation behavior was studied using DLS and continuously monitored phase-analysis light scattering (cmPALS), the latter being based on the electrophoretic light scattering technique. First, we measured DLS of all polymers in water in the same concentrations as in later EPR experiments. The mass-weighted size distributions thus determined are shown in **Figure 3**A; the respective autocorrelation functions are plotted in Figure S1 (Supporting Information). While SMA-SB and DIBMA show a steep intensity correlation function, indicating a unimodal and narrow size distribution, SMA behaved differently. For SMA, we found two populations below a hydrodynamic radius of 10 nm. By contrast, SMA-SB only exhibited one population between 1 and 10 nm, and DIBMA aggregated significantly more, which resulted in a hydrodynamic radius of ≈250 nm with only a small fraction of DIBMA forming aggregates of less than 50 nm in radius. For SMA-SB, a closer look at its temperature-dependent aggregation, thus, seemed necessary. SMA-SB is a zwitterionic sulfobetaine-containing polymer with an ammonium and a sulfonate moiety in each maleic amide monomer (Figure 1). Polymers of such structure tend to phase separate at lower temperatures, that is, they often possess an upper critical solution temperature (UCST), in water.[16,17] Below this temperature, the zwitterionic side chains of SMA-SB collapse due to intra- and intermolecular chain association and, thus, lose their water solubility.[16] This results in macroscopic phase separation in water which causes the intensity correlation function of SMA-SB to shift sharply to slower decay times (Figure S2, Supporting Information) and the transmission of the sample to drop (Figure 3B). Because of the sharp decrease in sample transmission with decreasing temperature, the UCST of those polymers correlates with a macroscopically observable cloud point.[17] Because of this UCST behavior of SMA-SB, we compare the light scattering results of DIBMA and SMA at 20 °C only with that of SMA-SB at 50 °C, that is, at a temperature above its cloud point.

Table 1. Properties of the studied nanodisc-forming polymers.

Polymer	Monomer ratio hydrophobic/hydrophilic	M_n [kDa]	Main interactions with nitroxide radicals
SMA	2.2:1	2.7[15]	Coulombic, hydrogen bonding, dipolar, π/π interactions
SMA-SB	2.2:1	4.15[a]	Coulombic, hydrogen bonding, dipolar, π/π interactions
DIBMA	1:1	8.4[9]	Coulombic, hydrogen bonding, dipolar, van der Waals interactions

[a] Estimated for full conversion of SMA.
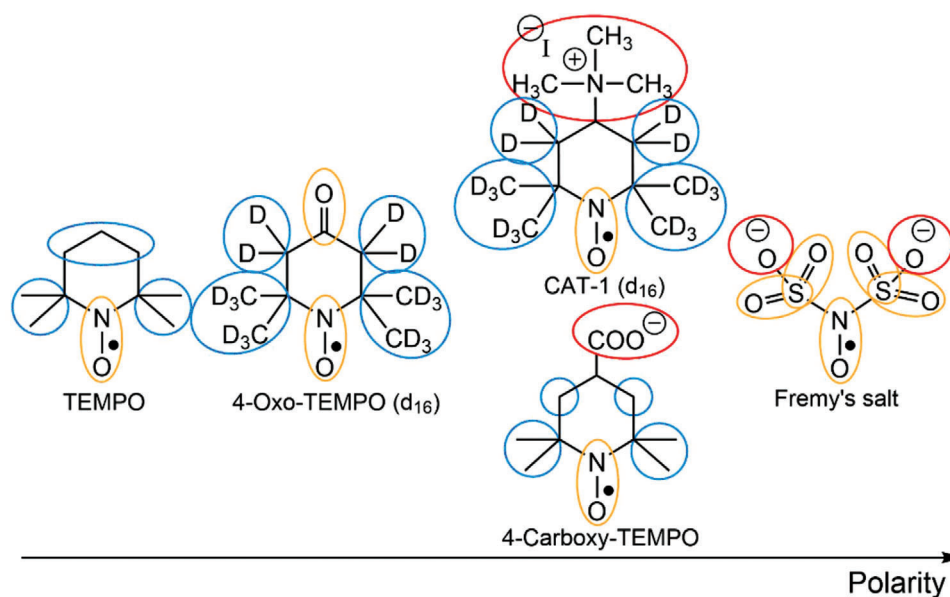
Figure 2. Comparison of chosen spin probes regarding their polarity and size, adapted from ref. [6]. The colors mark similar interaction sites as described in Figure 1.

For later application of these polymers in lipid particles, a purely aqueous system is not suited. Lipid solubilization is usually conducted at high ionic strength to decrease Coulomb repulsion between anionic lipids and polymers and to emulate more physiological conditions.[3,5] Therefore, we measured DLS of the polymers in saline Tris-buffered solution, as shown in Figure 3A and Figure S1 (Supporting Information). For all studied polymers in buffered solutions, a unimodal size distribution was observed with hydrodynamic radii below 10 nm. We did not perform temperature-dependent transmission measurements for SMA-SB in this system because the zwitterionic polymer did not exhibit any phase separation in the presence of the salt concentrations used.

DIBMA, SMA, and SMA-SB were then studied with electrophoretic light scattering to obtain insights into the effective charge in terms of the ζ potential on the polymers in solution. While SMA and DIBMA contain maleic acid moieties, these are completely amidated in SMA-SB. The observed ζ potentials are summarized in **Table 2**. From our results, it is evident that i) SMA and DIBMA possess much more negative ζ potentials than SMA-SB and ii) a higher ionic strength decreases the magnitude of the ζ potential of both anionic polymers. The latter observation stems from the adsorption of oppositely charged ions to the charged polymer surface as well as enhanced charge screening at elevated ionic strength. The difference in ζ potential between the two anionic polymers arises mainly from their differing particle size. DIBMA aggregates to form larger particles in both solvents compared to SMA, which presumably entails more extensive counterion adsorption and, thus, a decreased ζ potential. In addition, while the magnitude of the ζ potential of SMA and DIBMA decreases upon increasing the ionic strength, the ζ potential of SMA-SB turns from positive in water to negative in saline buffer. However, the UCST of SMA-SB did not vanish completely up to 100×10^{-3} M salt concentration.

2.2. Continuous-Wave Electron Paramagnetic Resonance Spectroscopy

The following sections highlight the results from the CW EPR measurements by first focusing on the interaction patterns for spin probes in the respective polymer mixtures at two different microwave frequencies. Afterwards, we discuss the effect of aqueous buffer solutions with high salt content, which are needed for the solubilization of lipids by the three polymers, on the respective noncovalent interactions as detected in the CW EPR spectra. At last, we present temperature-dependent measurements at X-band frequencies to especially study the UCST behavior of SMA-SB compared to the negatively charged SMA and DIBMA. The main EPR parameters that are used in the analysis are: i) the isotropic g-value, the fingerprint of the respective radical, that is also sensitive toward hydrogen bonding, ii) the isotropic ^{14}N hyperfine coupling constant a_{iso} that is a measure of the environmental polarity around the probe, and iii) the rotational mobility, in case of fast, rather isotropic rotation most simply described by the isotropic rotational correlation time τ_c.[11,18]

2.2.1. Interaction Patterns at X- and Q-Band Frequencies

Owing to their chemical structures, the applied spin probes report on different types of interactions in the presence of the respective systems of interest. These comprise as π/π interactions, hydrogen bonding, Coulomb, and dipole/dipole interactions as well as van der Waals and hydrophobic interactions.[19] The mono- and dianionic spin probes 4-carboxy-2,2,6,6-tetramethyl-1-piperidinyloxyl (4-carboxy-TEMPO) and disodium nitrosodisulfonate (Fremy's salt), respectively, as well as the cationic tetraalkylammonium TEMPO species (4-trimethylammonium-2,2,6,6-tetramethyl-1-piperidinyloxyl [CAT-1]) are able to participate in
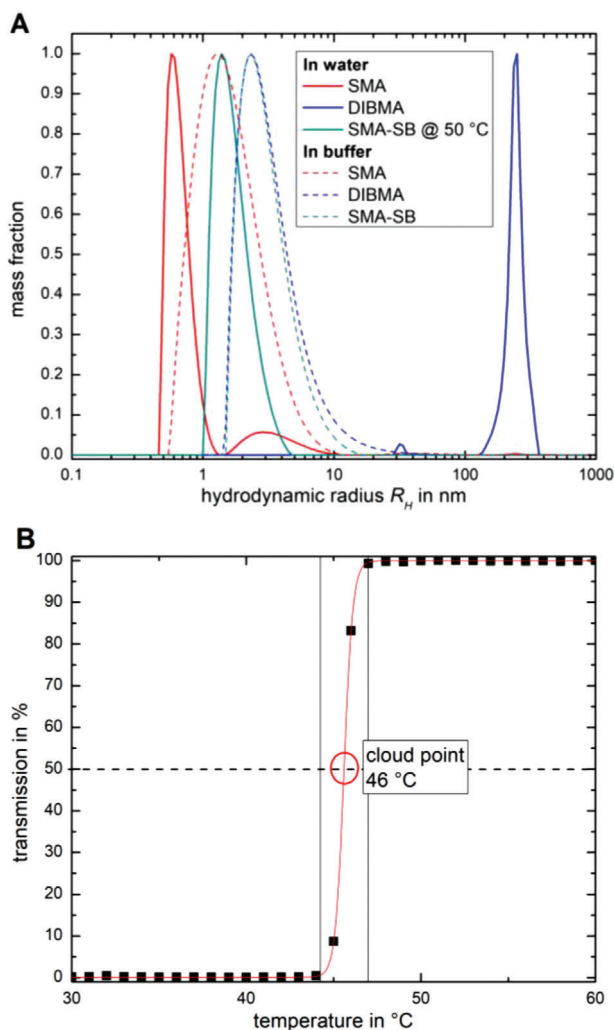
Figure 3. A) Mass-weighted particle size distribution for the pure polymer solutions of SMA and DIBMA, measured at 20 °C, and SMA-SB, shown at 50 °C (above its UCST) in water (solid lines) as well as in aqueous buffer solution (all measured at 20 °C, dashed lines). B) Temperature-dependent transmission of SMA-SB for cloud point determination.

strongly amphiphilic TEMPO can act as a dipolar molecule or interact via van der Waals contacts of its alkyl ring. This portfolio of readily available spin probes, thus, enables us to detect different modes of interactions between the studied polymers and small molecules using EPR spectroscopy.

The nitroxide-radical TEMPO bears no chemical modification at the 4-position of the piperidyl-ring and, hence, sets the reference point for our study. It is the most hydrophobic spin probe in our measurements but still owns an amphiphilic character with its rather large dipole moment ($\mu = 3.14$ D).[20,21] Note that this spin probe can neither form π-complexes with the styrene-unit in SMA and SMA-SB nor form Coulomb interactions with the polymer chains.

TEMPO: **Figure 4**A,B shows the CW EPR spectra for pure TEMPO in aqueous solution as well as with all the three polymers at both microwave frequencies. At X-band frequencies ($\nu \approx 9.4$ GHz), the values of the isotropic hyperfine coupling a_{iso} of the pure spin probe and in the polymer mixtures were not significantly different, indicating a similar polarity environment of the nitroxide radicals in all studied systems. The rotational mobility τ_c of TEMPO was only slightly affected by the presence of the polymers, as shown in Figure S3A and Table S2 (Supporting Information). The line width of the recorded spectra was larger for TEMPO dissolved in the presence of SMA-SB compared with the other samples. Note that we had to heat all SMA-SB samples above the UCST to fill the EPR capillaries and place them in the spectrometer. The actual measurement temperature of 20 °C was below the UCST of 46 °C, which promoted self-association and ion-pair formation among the zwitterionic side chains of SMA-SB, which, in turn, affected their interactions with the spin probe.[22,23] This self-association was also detected by DLS, as described in the previous section (Figure 3).

One significant change was visible for the isotropic g-value. TEMPO dissolved with SMA presented at X-band frequencies a much lower g_{iso}-value of 2.00555 compared with a pure aqueous spin probe solution (2.00587), while DIBMA and SMA-SB did not induce such a change. As there was no variation in a_{iso}, the drift in g_{iso} cannot be explained by simply invoking a more polar environment. Rather, it seems that the proticity of the spin probe was changed in response to the formation of hydrogen bonds between the oxygen of the nitroxide group and the two maleic acid units of SMA, of which approximately one is still protonated at pH 7.[24] The fact that the oxygen in N—O acts as a hydrogen bond acceptor decreases the variance between g_{xx} (and therefore g_{iso} due to $g_{iso} = \frac{1}{3}g_{xx} + g_{yy} + g_{zz}$)) and g_e for a free electron.[7] DIBMA did not show this effect, although this polymer also contains maleic acid

Coulomb interactions. Note that all ionic spin probes were used as salts, and we do not explicitly mention the respective counterions. 4-Oxo-2,2,6,6-tetramethyl-1-piperidinyloxyl (4-oxo-TEMPO), in turn, can interact with its carbonyl moiety via dipolar interactions and hydrogen bonding, while the

Table 2. Results of cmPALS. ζ potentials of SMA, DIBMA, and SMA-SB in water and buffer.

Polymers	H$_2$O		Tris buffer with 300×10^{-3} M NaCl	
	Hydrodynamic radius[a] [nm]	ζ potential [mV]	Hydrodynamic radius[a] [nm]	ζ potential [mV]
SMA	0.6	−52.0	2.2	−24.0
DIBMA	235.0	−36.3	3.7	−13.8
SMA-SB	1.7[b]	21.3	4.6	−10.8

[a] Calculated as weighted average from all sizes appearing in the mass-weighted size distribution; [b] Hydrodynamic radius of SMA-SB at 50 °C owing to phase separation occurring below the UCST at 46 °C.
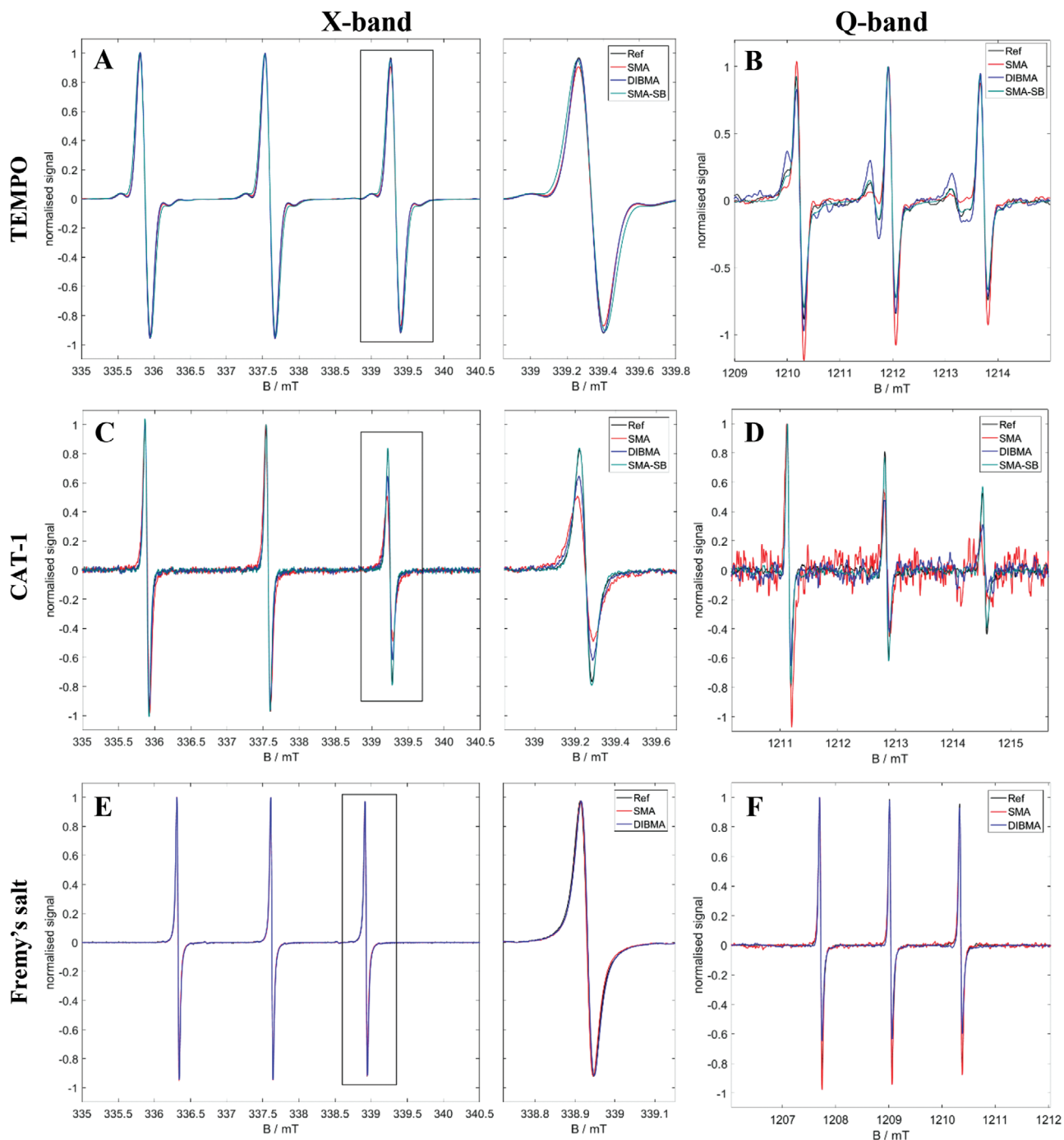
Figure 4. CW EPR spectra at 20 °C of A,B) TEMPO, C,D) CAT-1, and E,F) Fremy's salt in water (reference measurements) as well as with SMA, DIBMA, and SMA-SB, respectively. A,C,E) X-band spectra present the full spectra and highlight the high-field peaks. B,D,F) At Q-band frequencies, only full spectra are presented.

units. One reason could be that TEMPO prefers the region with the isobutylene units in DIBMA more but is still surrounded by enough water molecules to show a similar polarity profile compared to SMA with its styrene units based on the isotropic hyperfine coupling value, as schematically shown in Figure 9.

The Q-band spectra of TEMPO as spin probe presented one prominent feature that was not observed at lower microwave fre-

quency. Besides fully solvated molecules, amphiphilic TEMPO in water exhibits a second component representing radical molecules enclosed by a water solvation shell of significantly lower polarity and reduced rotational mobility (Figure S3B, Supporting Information). The cause for the formation of this second species containing an aqueous lower-polarity solvation shell (ALPSS) is described in a separate study.[21] Note that other

Table 3. Comparison of the fraction of the fully hydrated, "hydrophilic" TEMPO species (f) for each polymer as well as for pure TEMPO (Ref) in water at 20 °C.

Sample	Ref	SMA	DIBMA	SMA-SB
f [%]	76	88	65	70

nitroxide radicals such as 4-oxo-TEMPO (Figure S4, Supporting Information) do not exhibit this phenomenon. By using a higher magnetic field, the spectral resolution for parameters such as the **g**-tensor improves, thereby enabling a different view on rotational motion.[18,25] Here, we now focus on the ratio between these two different "types" of TEMPO species (ALPSS vs fully solvated) in the context of the three polymers tested. The fractions of the hydrophilic (i.e., fully solvated) spin probe as extracted from a simulation of the spectra (see the Supporting Information for further information), in each sample, are summarized in **Table 3**. Similar to the X-band results, it is evident that the SMA sample shows a different behavior compared with DIBMA and SMA-SB. The preferred formation of the hydrophilic TEMPO species in SMA can be correlated with the mentioned preference of the spin probe to interact with the maleic acid regime, whereas in DIBMA the isobutylene moiety is preferred (Figure 9). In SMA-SB, the polymer has the smallest effect on the population of the two TEMPO species. That fact agrees with the assumption that, below the UCST, the zwitterionic side chains interact more strongly with each other than with the nitroxide radical or any other guest molecules. Moreover, SMA-SB started to aggregate and precipitate inside the capillary directly after filling it with the preheated sample. By measuring it at room temperature (below UCST), mainly pure TEMPO radicals are left in solution.

Deuterated Nitroxide Radicals: For the spin probe 4-oxo-TEMPO, no significant differences when mixed with the three polymers were observed (Figure S4 and Table S3, Supporting Information).

Considering its charge and role as a strong electrolyte, the cationic nitroxide-radical CAT-1 may sample different environments when codissolved with the polymers mainly because of Coulomb interactions. The respective spectra at X- and Q-band frequencies are shown in Figure 4C,D. Note that we used fully deuterated CAT-1, which significantly reduced the line width of the recorded CW EPR data. The reason for this lies in a strong reduction of the unresolved hyperfine couplings arising from the methyl hydrogen nuclei.[26,27] When combining CAT-1 with SMA, the spectra at both microwave frequencies show reduced rotational mobility of the spin probe (visible in Figure S5, Supporting Information). The positively charged spin probe reveals rather strong Coulomb interactions with the negatively charged maleic acid regime of SMA, as depicted in Figure 9. The rotational correlation time for CAT-1 is roughly four times higher with polymer than in pure water (Table S4, Supporting Information). With DIBMA which also contains negatively charged maleic acid monomer units the mobility restrictions for CAT-1 were less pronounced. Here, τ_c rose by a factor of ≈ 2.2 only. This trend matches the determined ζ potential values from the cmPALS studies (Table 2), where SMA had a larger absolute value and, therefore, a more pronounced interaction with the

added spin probe. In addition, we ruled out any effect of the differing chain length of SMA and DIBMA by adjusting the polymer concentration to match a similar ratio of spin probe to mean repeat unit for all polymers, that is (styrene$_2$/maleic acid$_1$), (diisobutylene$_1$/maleic acid$_1$), and (styrene$_2$/maleic amide$_1$) for SMA, DIBMA, and SMA-SB, respectively. Zwitterionic SMA-SB did not affect the rotational behavior of CAT-1, which, again, correlates with the determined electrokinetic potential of this polymer. Moreover, it reinforces the interpretation that the polymer chains of SMA-SB prefer to electrostatically interact with each other below the UCST.

Negatively Charged Nitroxide Radicals: Similar to the neutral 4-oxo-TEMPO, negatively charged 4-carboxy-TEMPO (Figure S6, Supporting Information) shows no additional and significant changes in g_{iso} and a_{iso} in the recorded CW EPR spectra. Simply considering the charges, the spin probe should be repelled by SMA and DIBMA, which explains its unaltered mobility. For SMA-SB, the positively charged secondary ammonium region did not affect the rotational freedom of 4-carboxy-TEMPO. The self-association of the polymer below the UCST could prevent the spin probe to reach these positively charged regions on the polymer.

Besides 4-carboxy-TEMPO, we also used Fremy's salt as negatively charged and even dianionic spin probe. Note that this nitroxide radical does not contain a ring system like the TEMPO derivatives. The absence of other magnetic nuclei besides the nitrogen eliminates unresolved hyperfine couplings, which results in very narrow lines (Figure 4E,F). Because of the absence of a ring system and, therefore, the absence of methyl groups at positions 2 and 6, Fremy's salt is less stable than the other spin probes used.[20,28] To record X-band CW EPR spectra of Fremy's salt mixed with SMA-SB, several attempts were needed with focus on a fast transfer of the heated sample into the respective capillaries. In addition, we had to work above the UCST of SMA-SB to obtain a homogeneous sample, which was then cooled down just before measurements were performed. Because of the strong Coulomb interaction between the polymer and the nitroxide and a resulting increase in the local concentration of Fremy's salt (Figure 9 and Figure S7, Supporting Information), the disproportionation (as the main route of chemical decay, see ref. [28]) of the radical was promoted, leading to a reduced temperature stability up to roughly 40 °C (Figure S8, Supporting Information). The same strong dynamic electrostatic attachment[29,30] between Fremy's salt and SMA-SB resulted in distinct reduction of the rotational mobility of the spin probe. To simulate the recordable spectra of Fremy's salt, further investigations will be needed, which exceeds the scope of the present publication. The fact that this spin probe shows strong interactions with SMA-SB was supported by measurements in aqueous buffer solution (Section 2.2.2). For SMA and DIBMA, mixing the polymer with the spin probes did not require a heating process, so CW EPR spectra with Fremy's salt at both microwave frequencies could be measured. Similar to 4-carboxy-TEMPO, the rotational mobility of Fremy's salt is not affected by these polymers because of like-charge repulsion, again highlighted in Figure 9. The drop in g_{iso}, which was consistent for the TEMPO derivatives in SMA solution at X-band frequencies, does not appear for Fremy's salt (Table S6, Supporting Information). The dianionic character as well as the specific structure of this spin probe probably prevents

2100051 (6 of 14)

ADVANCED
SCIENCE NEWS
www.advancedsciencenews.com

Macromolecular
Chemistry and Physics
www.mcp-journal.de

its NO group from forming hydrogen bonds with the maleic acid residues.[31]

2.2.2. Influence of Saline Buffer Salts on the Interaction Patterns

As described above, near-physiological buffer and salt concentrations are needed for the solubilization of lipids by the three polymers. The effects of added buffer and salt on SMA, DIBMA, and SMA-SB were already discussed with the respective DLS and ELS measurements. Applying CW EPR spectroscopy, it is possible to distinguish between spin probe ensembles differing in their rotational time scale or polarity. Thus, we can now correlate variations in the local environment that can be discerned through different spectral components of the EPR spectra with values like the ζ potential that average over the complete ensembles of all types of molecules in the samples.

Similar to the spin probe measurements in water, we observed the most pronounced changes with the charged nitroxide radicals CAT-1 and Fremy's salt as well as with TEMPO and its specific solvation behavior (**Figure 5**). Note that 4-carboxy-TEMPO, which is also negatively charged, did not show significant changes in the recorded spectra at both X- and Q-band frequencies (Figure S12, Supporting Information). The unresolved hyperfine interactions for this specific spin probe led to larger line widths that largely impeded the resolution of spectral changes due to locally different interaction patterns.

For TEMPO, we focused on measurements performed at Q-band frequencies (Figure 5B), because they revealed the two differently solvated nitroxide species (Figure S9, Supporting Information, for all spectra). The addition of buffer salts destabilized the lower-polarity environment formed around the radical molecules by water, reducing the fraction of the ALPSS TEMPO species to 10%. Note that, by adding antichaotropic or kosmotropic compounds such as NaCl, one would induce the opposite effect[21] The polymers DIBMA and SMA-SB apparently did not disturb the overall buffer salt effect, presenting a similarly pronounced (i.e., small) ALPSS TEMPO component in the respective CW EPR spectra. However, SMA seemed to stabilize "hydrophobic" interactions in the aqueous buffer solution, increasing the fraction of ALPSS TEMPO to 40%. At this stage, it is hard to identify the main reason for the forced formation of the ALPSS TEMPO species. It could be that the high buffer salt content preferably interacts with the maleic acid residues in SMA, allowing TEMPO to be solvated in almost "pure" water regions that lead to ALPSS TEMPO species. It should be noted that the ALPSS TEMPO species observable at Q-band with the polymers was not due to direct interaction of TEMPO with the polymer, as we have frequently seen in thermoresponsive polymers[11] If these "more hydrophobic" species were due to polymer–TEMPO interactions, its mobility and relaxation would be such that it would show up at X-band frequencies, too. Because this was not the case, the polymer-induced shift in the ratio of "bulk" water to ALPSS water must have been a side effect of the added saline buffer. One may envisage that the presumably preferred interaction of buffer salts with the maleic acids of SMA also leads to a high concentration of ions close to the aromatic SMA rings that are adjacent to the maleic acid residues. Such, the ions may be seen as "shielding" the aromatic residues from TEMPO, too.

To obtain a better understanding of the accessibility of charged residues in DIBMA, SMA, and SMA-SB in saline Tris buffer solution, one, furthermore, needs to scrutinize the CW EPR spectra of CAT-1 (Figure S11, Supporting Information) and Fremy's salt (Figure S13, Supporting Information). The positively charged radical's rotational mobility was less restricted compared with the above measurements in water, when it was codissolved with SMA or DIBMA (Figure 5C,D). For these maleic acid-based polymers, τ_c decreased, based on the X-band results, by roughly 45% in the case of SMA and 31% for DIBMA. The added buffer salts partially screened the negative charge of both polymers, as already pictured in the less negative ζ potential values (Table 2), reducing the Coulomb interactions between the spin probe and the maleic acid residues. In solutions with DIBMA, CAT-1 was more mobile, which also correlates with the above electrokinetic potential. As SMA-SB also possesses a negative ζ potential in the aqueous Tris buffer solution, the rotational mobility of CAT-1 was reduced in buffered SMA-SB solutions as well. However, its influence was even less pronounced than in case of DIBMA.

One major advantage of using high salt concentrations is the vanishing of the UCST behavior of SMA-SB as a consequence of charge screening. Buffered SMA-SB solutions, hence, did not have to be heated up to obtain a homogeneous solution, allowing us to record CW EPR spectra with Fremy's salt with sufficient signal-to-noise ratio (compare Figure 5E,F with Figure S8A, Supporting Information). As expected, the positively charged ammonium moiety in SMA-SB electrostatically interacted with the negatively charged nitroxide radical, thereby reducing its rotational mobility. Note that this hindered mobility was visible only at X-band frequencies. At higher frequencies (Q-band), the apparent rotational correlation times for Fremy's salt were the same with and without polymer. This indicates a rather dynamic attachment, similar to a "territorially bound" ion as described in the concept of counterion condensation introduced by Manning that could be measured and quantified by EPR spectroscopy.[29,30,32] Please note that due to the rather loose and dynamic attachment of the guest molecules, we do not expect that separation methods are able to remove "free" spin probe. In this case, we would remove all the spin probes or enough radical molecules to result in spectra below the detection limit of the applied method. For SMA and DIBMA, the mobility of the nitroxide radical was unaffected because of the Coulomb repulsion between both components.

2.2.3. Influence of Temperature on Spin Probe Parameters

In the following, we discuss the temperature dependence of the CW EPR spectra of the nitroxide spin probes in all polymer solutions. In doing so, we focus on the measurements of aqueous samples at X-band frequencies (Figures S14–S21, Supporting Information). Note that the respective spectra in aqueous buffer solution can be found in Figures S22–S31 (Supporting Information). SMA-SB is a UCST polymer, i.e., it is macroscopically dissolved in a single phase above but precipitates below its phase transition temperature. At the critical solution temperature of SMA-SB, the polymer side chains unfold from their aggregated state, and the intramolecular ion pairs are broken up to form dissolved coils capable of interacting with small molecules in the solution. The cloud point observed by EPR spectroscopy
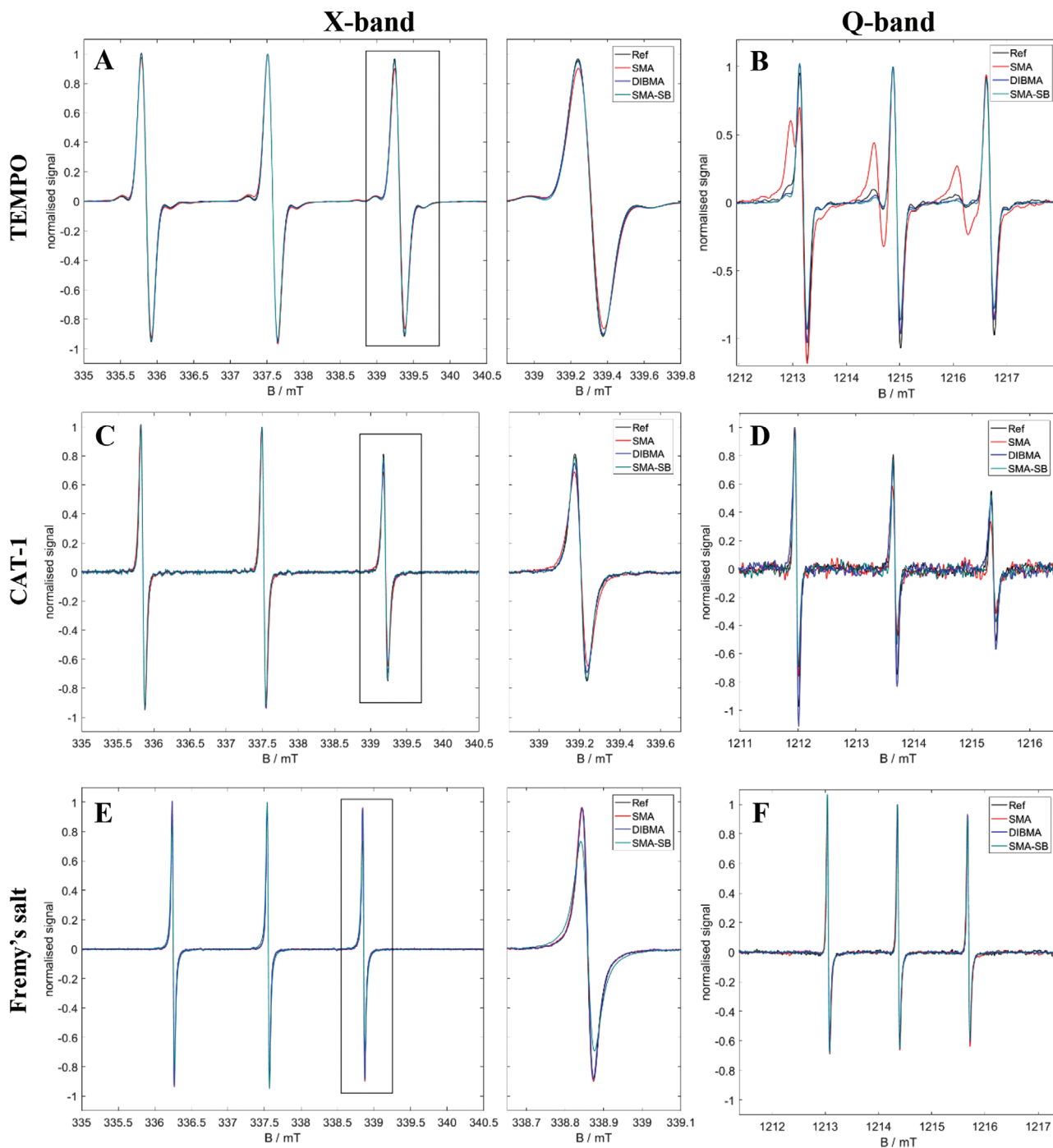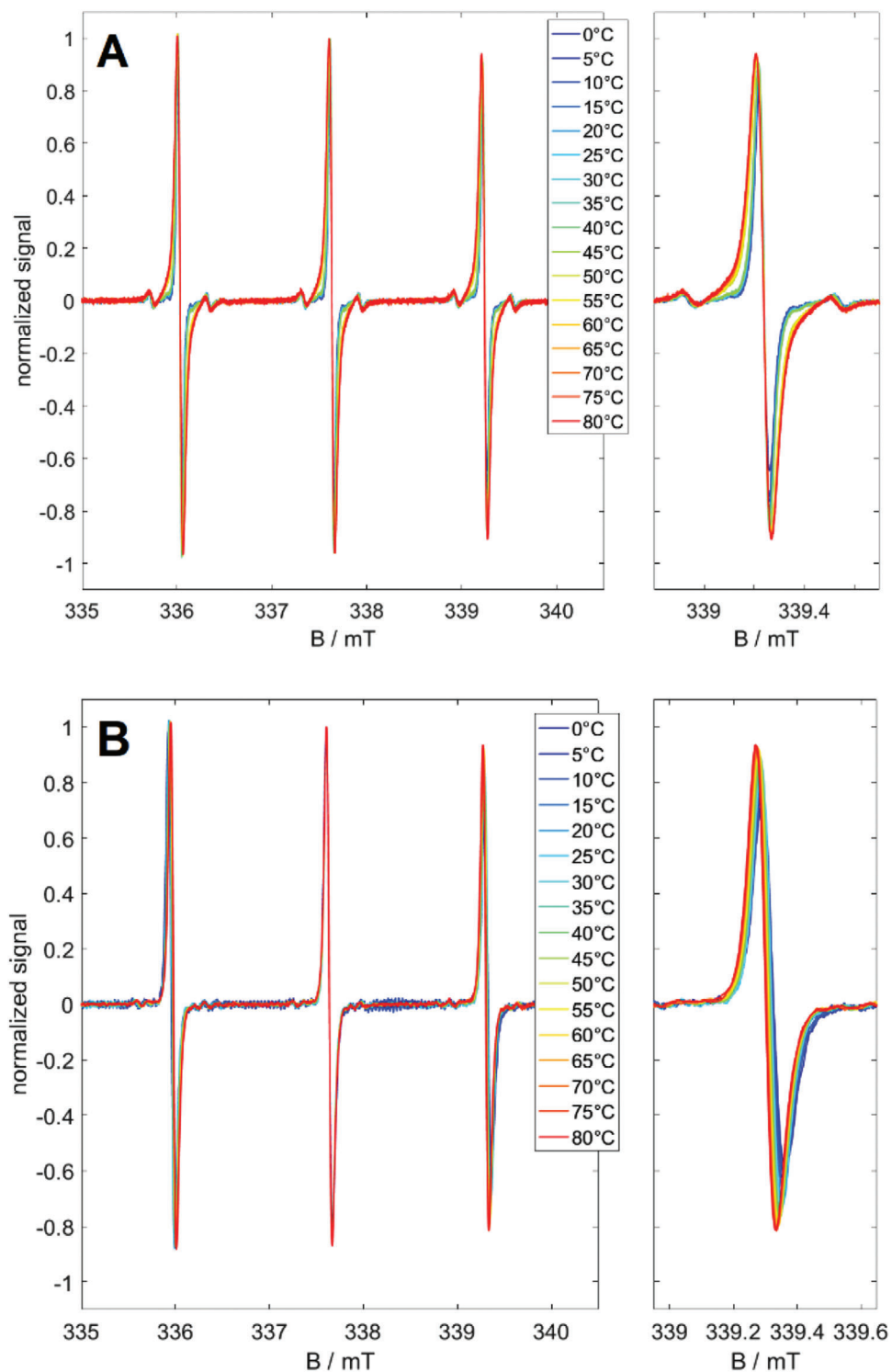
Figure 5. CW EPR spectra at 20 °C of A,B) TEMPO, C,D) CAT-1, and E,F) Fremy's salt in aqueous buffer solution as well as with SMA, DIBMA, and SMA-SB, respectively. A,C,E) X-band spectra present the full spectra and highlight the high-field peaks. B,D,F) At Q-band frequencies, only full spectra are presented.
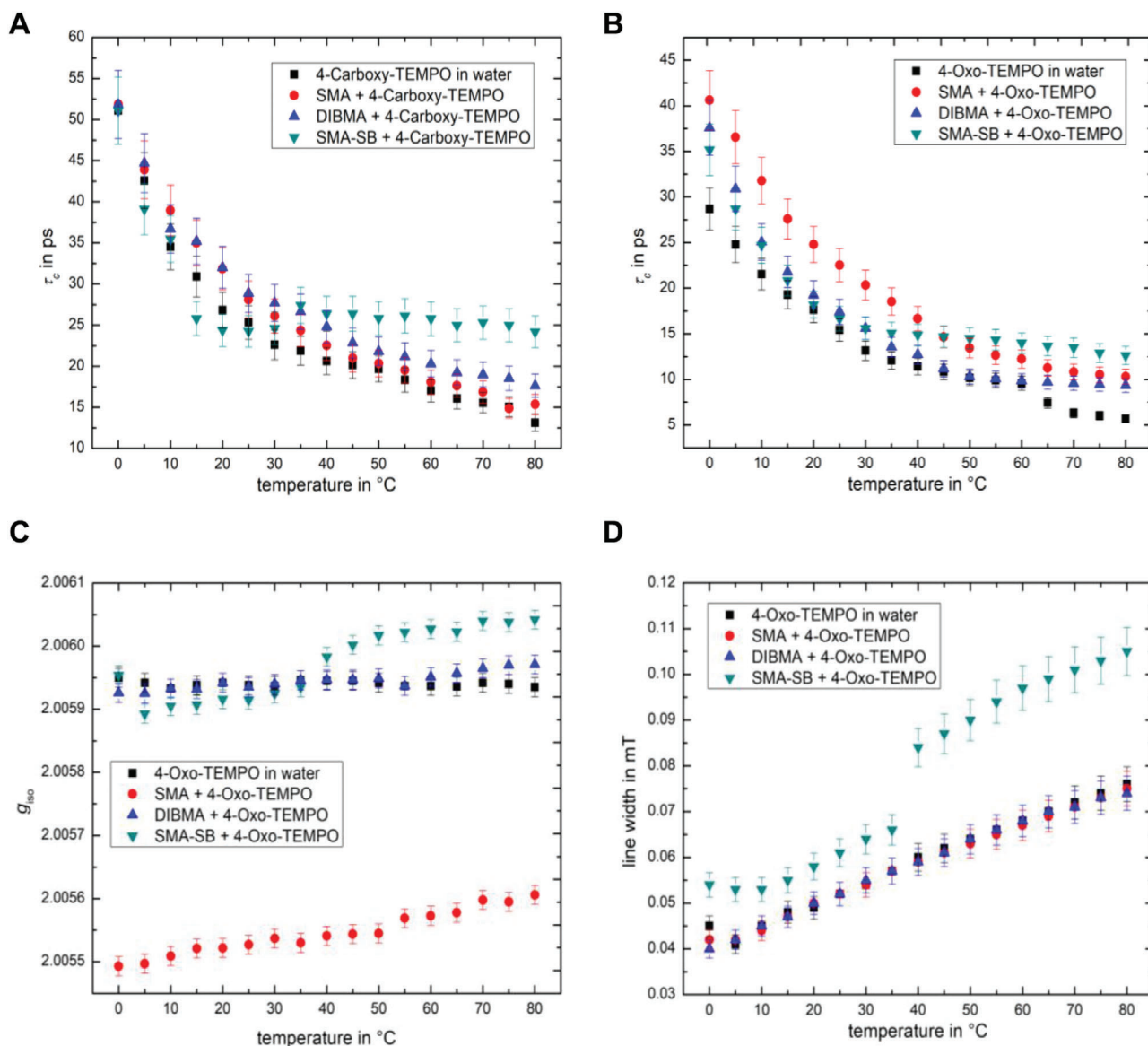
enabled detection of the nanoscopic side chain unfolding of the polymer at lower temperatures than visible in DLS.[14] We are able to detect the opening of SMA-SB from its aggregated to its soluble form, we also observe temperature-dependent changes in the interaction patterns between the applied spin probes and the polymers SMA and DIBMA. In **Figure 6** CW EPR spectra of 4-oxo-TEMPO and CAT-1 in aqueous solution containing SMA-

SB at selected temperatures are shown, which in combination with the data presented in the Supporting Information are the basis of the following plots.

The spectra show a temperature-induced line broadening that is most prominent for the high-field peak and is not the result of spin probe degradation (Figures S24 and S25, Supporting Information). The line broadening is more pronounced for

ADVANCED
SCIENCE NEWS

www.advancedsciencenews.com

Macromolecular
Chemistry and Physics

www.mcp-journal.de

Figure 6. Temperature-dependent X-band CW EPR spectra of A) 4-oxo-TEMPO and B) CAT-1 with SMA-SB. On the right-hand side, the high-field peak is shown separately.

**ADVANCED
SCIENCE NEWS**

www.advancedsciencenews.com

**Macromolecular
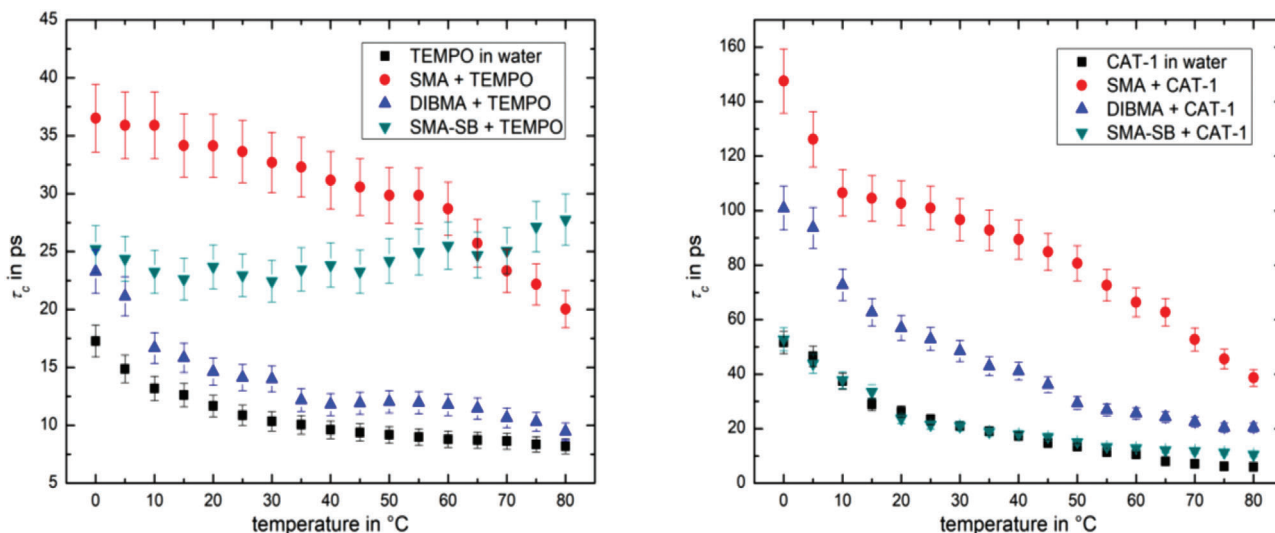Chemistry and Physics**

www.mcp-journal.de

Figure 7. Results of spectral simulations of temperature-dependent CW EPR spectra measured at X-band frequencies of A) 4-carboxy-TEMPO and B–D) 4-oxo-TEMPO with all polymers in water. Temperature dependencies of A,B) τ_c, C) g_{iso}, and D) the line width.

4-oxo-TEMPO than for CAT-1. Overall, all spectra show largely isotropic character (e.g., the almost equal line heights) with slightly larger anisotropy for CAT-1. Hence, we conclude that 4-oxo-TEMPO weakly interacts with the polymer, whereas the positively charged nitroxide radical does not. This was further supported by simulating the temperature-dependent spectra and obtaining τ_c which suggests a more confined rotation than observed in freely rotating 4-oxo-TEMPO. However, the calculated τ_c-value is much lower than for polymer-attached nitroxide radicals (**Figure 7**B). For CAT-1, the rotational mobility was not affected by SMA-SB (**Figure 8**B), as discussed next.

In the case of 4-oxo-TEMPO without polymer, the line width slowly increased with rising temperature, as shown in Figure 7D, as we would expect due to more frequent intermolecular collisions.[14] Similar results were seen when 4-oxo-TEMPO was

mixed with SMA or DIBMA. Only the mixture of SMA-SB and 4-oxo-TEMPO behaved differently, as at 40 °C we observed a sharp rise in line width by 0.015 mT, slightly below the macroscopic transition temperature of ≈46 °C.

A similar effect was found for g_{iso} at 40 °C, where we observed a turning point of g_{iso} for the ketone-bearing spin probe with SMA-SB (Figure 7C). Compared with the steady increase detected in the mixture with SMA, this change could be correlated with the chemical modification of SMA-SB. There is a clear change in hydrophobicity resulting in differences in g_{iso}. Especially g_{iso} of 4-oxo-TEMPO when mixed with SMA decreased compared to the systems with DIBMA, SMA-SB, or free spin probe. For SMA we deduce that the probe is located in the boundary layer between SMA and bulk water; therefore, it senses a more hydrophobic environment closer to the polymer chain. The amphiphilic side

**ADVANCED
SCIENCE NEWS**

www.advancedsciencenews.com

**Macromolecular
Chemistry and Physics**

www.mcp-journal.de

Figure 8. Temperature-dependent τ_c measured at X-band frequencies of A) TEMPO and B) CAT-1 in all studied systems in water.

chains of SMA-SB participate in the hydrogen bonding network and, therefore, influence the adjacent water molecules. However, SMA-SB can exert this effect only above the nanoscopic cloud point of 4-oxo-TEMPO at 40 °C.

Also included in Figure 7A is 4-carboxy-TEMPO, an anionic spin probe, which should be capable of interacting with the positively charged ammonium groups owing to attractive electrostatic forces. In the measurement series of 4-carboxy-TEMPO, we also find a τ_c difference between SMA-SB and the other polymers. The spin probe without polymer as well as in its mixtures with SMA and DIBMA reveals a decrease in τ_c with increasing temperature. A drop in τ_c is the result of a faster rotation of the probe or the polymers associated with it. τ_c of 4-carboxy-TEMPO/SMA-SB showed a kink beginning at 25 °C. With this spin probe, we also observed a cloud point of SMA-SB as seen from the nanoscopic/molecular point of view. This temperature is much below the macroscopically observed cloud point indicating that the sulfobetaine side chains start to interact with the environment or directly with the probe at this temperature already. It should be noted that the spin probe is only "territorially" bound;[29] in case of a directly bound probe, τ_c would be significantly larger due to the transient immobilization.
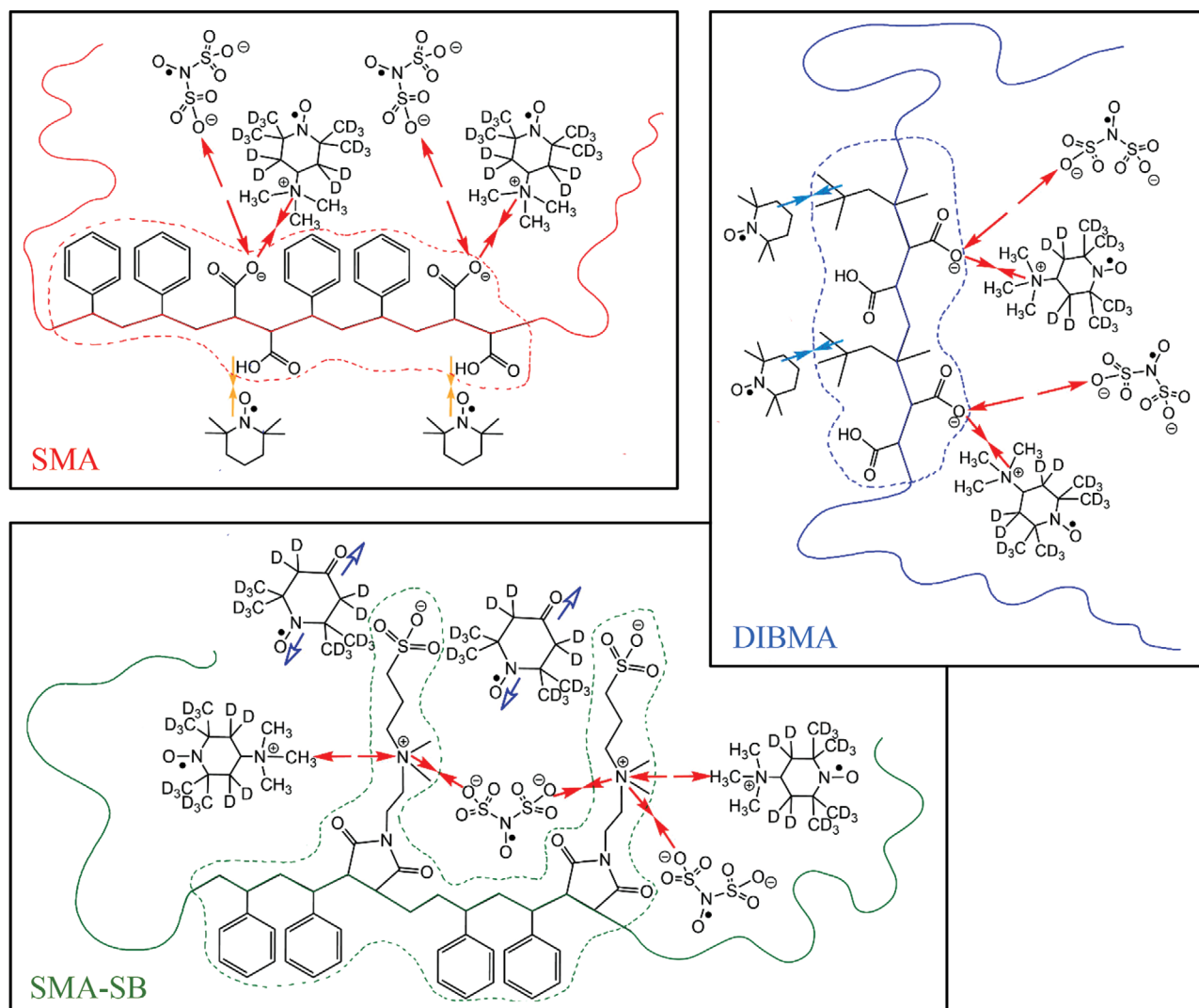
CAT-1 completes the small-molecules' view on the polymers. It is the only cationic probe used and in comparison with 4-carboxy-TEMPO, CAT-1 shows hardly any attractive interactions with SMA-SB. Apparently, the repulsion of the cationic groups of spin probe and polymer exceeds a possible attraction of cationic spin probe and anionic sulfonate groups within the polymer. This can be seen in Figure 8B, as the τ_c of CAT-1/SMA-SB decreases in a similar way to that of free CAT-1. By contrast, the interactions between CAT-1 and DIBMA or SMA are noteworthy. Both still have freely accessible maleic acid groups leading to a higher τ_c than that of free CAT-1 (Figure 8B, 100–150 and 60–100 ps for CAT-1 with SMA and DIBMA, respectively); here, we also interpret these results in the context of "territorially" bound probes.

TEMPO is the last probe used for the temperature-dependent measurements. As reflected in its large octanol/water partition coefficient,[33] TEMPO has the capability to detect hydrophobic

regions as shown in previous studies.[11,21] While free TEMPO as well as TEMPO mixed with DIBMA show small τ_c values that further decrease rapidly with increasing temperature, with SMA it shows a significantly higher τ_c at low temperatures. The hydrophobic phenyl groups of SMA may present hydrophobic "pocket" regions to which TEMPO may be associated, in contrast to the diisobutylene moieties of DIBMA. Below 60 °C, these pockets seem quite stable, as τ_c only decreases by 7 ps within this temperature range, indicating continuing immobilization despite increasing thermal energy. However, above 60 °C these hydrophobic regions seem to break down for TEMPO, which could have two causes: i) the decreasing polarity[14] of water causes the polymer to present its hydrophobic pockets to the outside, or ii) because of increasing kinetic energy and resulting side chain movements, the formation and survival of hydrophobic pockets become harder. The opposite effect was found for the development of τ_c for SMA-SB. Initially, τ_c plateaus at 25 ps but starts to rise at 60 °C. In the context of the other spin probes, TEMPO does not evidence a nanoscopic cloud point but could still interact with the phenyl groups inside the polymer's side chains, especially at higher temperatures, that is, above the macroscopic cloud point.

3. Conclusion

By applying continuous-wave EPR spectroscopy, we have demonstrated that the three nanodisc-forming polymers SMA, DIBMA, and SMA-SB exhibit polymer-specific noncovalent interaction patterns with nitroxide radicals. To separate different types of noncovalent interactions (such as ionic interactions or dipole/dipole interactions), we used a variety of spin probes with different chemical structures and functionalities. The respective main interaction patterns between the chosen spin probes and the polymers, which we dissected with the aid of CW EPR spectroscopy, are highlighted in **Figure 9**. Furthermore, the locally resolved structural and dynamic properties of the polymers could be correlated with the previously categorized ensemble-averaged parameters such as the hydrodynamic radius and the ζ potential

ADVANCED
SCIENCE NEWS
www.advancedsciencenews.com

Macromolecular
Chemistry and Physics
www.mcp-journal.de

Figure 9. Schematic representation of the main interaction patterns between selected nitroxide radicals and the three studied polymers SMA, DIBMA, and SMA-SB as found in this study. The colors of the arrows that visualize attractive or repulsive forces (as indicated by their directions) match those in Figure 1. Red, ionic interactions; yellow, hydrogen bonding and dipole/dipole interactions; dark blue, π/π interactions; light blue, van der Waals interactions.

determined with DLS and ELS, respectively. The major conclusions can be formulated as follows:

- SMA-SB possesses an UCST in water at 46 °C, with macroscopic phase separation taking place below this temperature.
- The electrokinetic potential of the polymers can predict the kinds of interactions expected with other molecules, with aqueous buffer solutions influencing this effect.
- In SMA and DIBMA, ionic interactions dominate the interaction patterns with other molecules. For SMA-SB with its zwitterionic side chains, weaker noncovalent interactions such as hydrophobic forces have to be accounted for dominant interaction patterns to describe the rather dynamic assembly with guest molecules such as Fremy's salt.
- Temperature-dependent CW EPR measurements allow the characterization of nanoscopic cloud points depending on the

interaction patterns between SMA-SB and a spin probe, which can occur more than 20 °C below the macroscopically observed UCST.

The differences observed among the interaction patterns of DIBMA, SMA, and SMA-SB will be useful in future studies to understand the interplay between these polymers and other small- to medium-sized molecules, most notably, membrane lipids and proteins. Interactions between lipids and the three polymers will be presented in a following study using spin-labeled lipids embedded in a DMPC model membrane. Finally, the good agreement between the chemical structures of the spin probes used in this study and their differential interactions with the three polymers may prove useful for designing new polymers with improved lipid solubilization and protein-extraction properties to form native-like nanodiscs.

4. Experimental Section

Materials: DIBMA (poly-diisobutylene-*alt*-maleic acid; Sokalan CP 9) was kindly provided by BASF (Ludwigshafen, Germany). SMA (2:1) (poly-styrene-maleic acid; tradename Xiran SZ30010) was a kind gift from Polyscope (Geleen, Netherlands). SMA-SB (poly-styrene-maleic-amide sulfobetaine) was synthesized from styrene/maleic anhydride (2:1) reacting with *N*,*N*-dimethylethylenediamine to form a maleimide which was further reacted with propane sultone to afford the final product. Buffer salts were obtained from Carl Roth (Karlsruhe, Germany, Tris buffer salt >99.3% and NaCl > 99.7%). Spin probes were obtained from commercial sources and used without further purification: TEMPO > 99% (Aldrich, St. Louis, MO), deuterated 4-oxo-TEMPO > 97% D (Isotec, Miamisburg, OH), 4-carboxy-TEMPO > 97% (Sigma Aldrich, St. Louis, MO), Fremy's salt (Aldrich, St. Louis, MO), and deuterated CAT-1 > 98%) CDN Isotopes, Quebec, Canada).

Preparation of Polymer and Spin Probe Solutions: Polymer solutions were prepared by dissolving an appropriate amount in either water (Millipore MilliQ water with a specific resistance of $\rho = 18.2$ MΩ cm) or Tris buffer (50 × 10^{-3} M Tris, 300 × 10^{-3} M NaCl, pH 7.4) to yield mass concentrations of 25 mg mL^{-1} (DIBMA and SMA) or 15 mg mL^{-1} (SMA-SB) at room temperature followed by heating combined with ultrasonicating for 30 min at 70 °C. During preparation, polyanionic SMA and DIBMA dissolved readily in both solvents, whereas zwitterionic SMA-SB dissolved slowly. After cooling down, DIBMA and SMA (2:1) stock solutions (and SMA-SB dissolved in Tris buffer) were stable for two weeks if stored at room temperature; by contrast, SMA-SB in water phase-separated below its UCST. A similar observation was previously made for other sulfobetaine polymers.[17] Samples were prepared from stock solutions by diluting them to monomer concentrations of 75 × 10^{-3} M. For EPR measurements, spin probe stock solutions of 6 × 10^{-3} M spin probe were added to yield a final spin probe concentration of 150 × 10^{-6} M at a spin/monomer ratio of 1:500 (mol/mol). Because SMA-SB did not dissolve in an amount sufficient for 75 × 10^{-3} M monomer, the respective approaches were scaled down to 134 × 10^{-6} M spin probe and ≈28.3 × 10^{-3} M monomer to ensure an appropriate spin/monomer ratio as well as a sufficient signal/noise ratio.

Light Scattering: DLS experiments were conducted on a Litesizer 500 (Anton Paar, Graz, Austria) equipped with a Micro Quartz cuvette with a sample capacity of 70 µL. The sample was irradiated at $\lambda = 658$ nm, and side scattering (90°) was measured at constant temperature. Prior to each measurement, the sample was allowed to equilibrate for at least 1 min. DLS data were evaluated with the Contin algorithm[34] applying the ALV-5000/E/EPP software (v. 3.0.1.13, ALV Laser-Vertriebsgesellschaft Langen, Germany). cmPALS was performed with the same system using the Univette (Anton Paar). Each experiment was conducted at least three times to ensure reproducibility with an equilibration time of 1 min prior to each repetition. Electrophoretic mobilities were averaged, and ζ potentials were calculated as detailed in the Supporting Information.

CW EPR Spectroscopy: CW EPR at X-band frequencies was carried out on the Miniscope MS5000 (magnettech, Freiberg, Germany) benchtop spectrometer. To perform temperature-dependent measurements, the device was connected to a temperature controller H04 (magnettech). All spectra were recorded with a magnetic field sweep of 10 mT centered around 337.5 mT, a scan time of 60 s, a modulation amplitude of 0.02 mT, and a microwave attenuation of 15 dB, corresponding to a microwave power of 3.16 mW. For the measurements at Q-band frequencies, a Bruker EMX-plus Q spectrometer with an ER5106QT resonator (Bruker Biospin, Rheinstetten, Germany) was used. To record the respective room-temperature spectra, most of the parameters were copied from the X-band measurements. Note that the modulation amplitude was chosen as 0.05 mT for TEMPO and 4-carboxy-TEMPO, whereas for 4-oxo-TEMPO, CAT-1, and Fremy's salt it was reduced to 0.02 mT. Please note that the reduced modulation amplitude decreases the absolute signal intensity and respective signal-to-noise ratio.

The sample preparation routine was similar for both frequencies. Moreover, the same batch of prepared samples were measured, leading to unavoidable storage time for the samples. The storage period could affect some of the samples in a profound way. Fremy's salt samples needed to prepared freshly owing to its less stability compared to the TEMPO-based nitroxide radicals. Micropipettes (BLAUBRAND intraMARK, Wertheim, Germany) were filled with 10–15 µL sample and capped with capillary tube sealant (CRITOSEAL Leica). Spectral simulations were performed in MatLab (R2016a, v. 9.0) in combination with the EasySpin package for EPR spectroscopy (v. 5.2.25).[35] For better comparison, the presented figures with CW EPR spectra are superimposed at the center field position.

Conflict of Interest

The authors declare no conflict of interest.

Author Contributions

J.E., M.H., and F.A.S. contributed equally to this work. J.E., M.H., F.S., C.V., S.K., and D.H. conceived and planned research; J.E. and M.H. contributed to sample preparation; J.E., M.H., and F.S. performed experiments; M.D. carried out polymer synthesis; J.E., M.H., F.S., C.V., S.K., and D.H. analyzed data; J.E. and F.S. carried out spectral simulations; J.E., M.H., F.S., C.V., S.K., and D.H. wrote the publication.

Data Availability Statement

Research data are not shared.

[1] S. C. Lee, N. L. Pollock, *Biochem. Soc. Trans.* **2016**, *44*, 1011
[2] M. Overduin, M. Esmaili, *SLAS Discovery* **2019**, *24*, 943.

[3] J. M. Dörr, S. Scheidelaar, M. C. Koorengevel, J. J. Dominguez, M. Schäfer, C. A. Van Walree, J. A. Killian, *Eur. Biophys. J.* **2016**, *45*, 3.

[4] N. Österlund, J. Luo, S. K. T. S. Wärmländer, A. Gräslund, *Biochim. Biophys. Acta, Proteins Proteomics* **2019**, *1867*, 492.

[5] S. Scheidelaar, M. C. Koorengevel, J. D. Pardo, J. D. Meeldijk, E. Breukink, J. A. Killian, *Biophys. J.* **2015**, *108*, 279.

[6] G. Jeschke, *Macromol. Rapid Commun.* **2002**, *23*, 227.

[7] *Advanced ESR Methods in Polymer Research* (Ed: S. Schlick), Wiley-Interscience, New Jersey **2006**.

[8] D. Hinderberger, in *EPR Spectroscopy – Applications in Chemistry and Biology* (Eds: M. Drescher, G. Jeschke), Springer-Verlag, Berlin **2012**, pp. 67–89.

[9] A. O. Oluwole, B. Danielczak, A. Meister, J. O. Babalola, C. Vargas, S. Keller, *Angew. Chem., Int. Ed.* **2017**, *56*, 1919.

[10] A. O. Oluwole, J. Klingler, B. Danielczak, J. O. Babalola, C. Vargas, G. Pabst, S. Keller, *Langmuir* **2017**, *33*, 14378.

[11] D. Kurzbach, M. J. N. Junk, D. Hinderberger, *Macromol. Rapid Commun.* **2013**, *34*, 119.

[12] U. Cerajewski, J. Träger, S. Henkel, A. H. Roos, M. Brehm, D. Hinderberger, *Phys. Chem. Chem. Phys.* **2018**, *20*, 29591.

[13] H. H. Haeri, J. Blaffert, F. A. Schöffmann, M. Blech, J. Hartl, P. Garidel, D. Hinderberger, *Molecules* **2019**, *24*, 2528.

[14] J. Hunold, T. Wolf, F. R. Wurm, D. Hinderberger, *Chem. Commun.* **2019**, *55*, 3414.

[15] A. Grethen, A. O. Oluwole, B. Danielczak, C. Vargas, S. Keller, *Sci. Rep.* **2017**, *7*, 1.

[16] J. Seuring, S. Agarwal, *Macromol. Rapid Commun.* **2012**, *33*, 1898.

[17] J. Niskanen, H. Tenhu, *Polym. Chem.* **2017**, *8*, 220.

[18] H. J. Steinhoff, *Supramol. Struct. Funct.* **2005**, *8*, 157.

[19] T. Hauenschild, D. Hinderberger, *ChemPlusChem* **2019**, *84*, 43.

[20] E. G. Rozantsev, *Free Nitroxyl Radicals*, **1970**.

[21] J. Hunold, J. Eisermann, M. Brehm, D. Hinderberger, *J. Phys. Chem. B* **2020**, *124*, 8601.

[22] L. Chen, Y. Honma, T. Mizutani, D.-J. Liaw, J. P. Gong, Y. Osada, *Polymer* **2000**, *41*, 141.

[23] Y. Kotsuchibashi, *Polym. J.* **2020**, *52*, 681.

[24] S. Scheidelaar, M. C. Koorengevel, C. A. Van Walree, J. J. Dominguez, J. M. Dörr, J. A. Killian, *Biophys. J.* **2016**, *111*, 1974.

[25] D. Hinderberger, G. Jeschke, in *Modern Magnetic Resonance* (Ed: G. A. Webb), Springer, Dordrecht, The Netherlands **2008**, pp. 1529–1537.

[26] A. H. Beth, R. C. Perkins, S. D. Venkataramu, D. E. Pearson, C. R. Park, J. H. Park, L. R. Dalton, *Chem. Phys. Lett.* **1980**, *69*, 24.

[27] J. H. Park, W. E. Trommer, in *Spin Labeling Theory and Applications* (Eds: L. J. Berliner, J. Reuben), Springer US, Boston, MA **1989**, pp. 547–595.

[28] A. Morante, R. Forteza, V. Cerdá, V. CerdÁ, *Thermochim. Acta* **1987**, *118*, 215.

[29] D. Hinderberger, H. W. Spiess, G. Jeschke, *Europhys. Lett.* **2005**, *70*, 102.

[30] G. S. Manning, *Eur. Phys. J. E* **2011**, *34*, 132.

[31] J. Heller, H. Elgabarty, B. Zhuang, D. Sebastiani, D. Hinderberger, *J. Phys. Chem. B* **2010**, *114*, 7429.

[32] D. Hinderberger, H. W. Spiess, G. Jeschke, *Appl. Magn. Reson.* **2010**, *37*, 657.

[33] L. J. Kirschenbaum, P. Riesz, *Ultrason. Sonochem.* **2012**, *19*, 1114.

[34] S. W. Provencher, *Comput. Phys. Commun.* **1982**, *27*, 213.

[35] S. Stoll, A. Schweiger, *J. Magn. Reson.* **2006**, *178*, 42.